

High Frequency Vector Sensor Design and Testing

W.W. Lee, M. Parent, and G. San Antonio
Radar Division

Introduction: An electromagnetic vector sensor (EMVS) is a complex antenna; it measures the three orthogonal components of the electric field in addition to the three components of the magnetic field at a single point.^{1,2} It is sensitive to both the direction-of-arrival and polarization of incoming electromagnetic waves. While the use of traditional antennas and antenna arrays for direction-of-arrival estimation/beamforming is well understood, the EMVS provides new potential applications and fresh challenges. The design and construction of a structurally sound EMVS for high-frequency (HF) skywave applications opens the door to further explore ionospheric and signal processing possibilities utilizing the additional information provided by the EMVS antennas.

Relevance: Ground-based radar systems that survey vast areas and operate over large distances are tasked to detect small targets thousands of kilometers away. Radio waves tend to travel in straight lines, limiting detection to objects above the horizon, due to the curvature of the Earth. Over-the-horizon radar systems use radio signals that are transmitted skyward and refracted toward the ground by the ionosphere to get energy to and from targets beyond the horizon.

The ionosphere is a dynamic channel and thus target geolocation and detection is subject to precise characterization of the propagated HF signals. The development and understanding of advanced HF antennas are essential in accurately understanding the state of the ionospheric channel path and its effect on radio frequency (RF) signal refraction and subsequent changes in polarization. To this end, the Radar Division at the Naval Research Laboratory has built and experimentally tested a novel EMVS design for use in the HF band (3 to 30 MHz).

Construction: EMVS antennas provide more information than traditional whip antennas. A single vertical monopole antenna has an azimuthally equal omnidirectional radiation pattern with a minimum at its zenith. The Radar Division–designed EMVS consists of three orthogonally oriented electrically short dipoles and three electrically small orthogonal loop elements (Fig. 1). The EMVS uses active electronic circuits to force the unbalanced coax transmission line to properly feed the balanced loops and dipoles. As such, a power source is required to operate the EMVS. The loop electronic components are independently housed at the

base of each orthogonal loop while electronics for all dipoles are housed in a sphere at the co-located center of the EMVS.

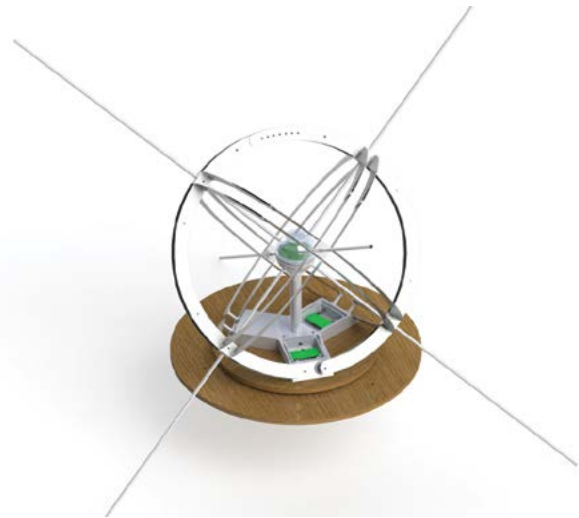


FIGURE 1

The electromagnetic vector sensor consists of three loops and three dipoles. Antenna electronics are shown in green. An “active balun” is housed at the base of each loop, while circuitries for the dipoles are housed together in the center sphere. The loops are 3 ft in diameter while the dipole elements are 8 ft from end to end.

A single EMVS can be considered to be composed of six independent antennas. The three loop components are used primarily to sense magnetic fields while the three dipoles act like traditional short dipole antennas and primarily sense the electrical fields. Careful consideration in the design is given to the structural stability, isolation, and symmetry of the sensor. A twin loop antenna design is adopted so that at joints where two twin loop antennas intersect, a dipole antenna can be inserted between with an insulated nylon block. In addition, the twin loop design widens the bandwidth response from the loop elements. This provides support for the loop intersection joint as well as durability for the dipole. Nylon construction components are used to minimize coupling effects between the antenna elements. Experimental measurements show the components to be sufficiently decoupled for purposes of directional wave analysis in spite of their relatively close electrical spacing.

The orthogonal sets of loop and dipole antennas are initially oriented with dipole elements directed along the x-y-z axes of the Cartesian coordinate system. This is then rotated along the z and y axes to create a symmetric response (with respect to the ground) from individual field sensing components due to ground interaction and reduce the signal processing requirements.

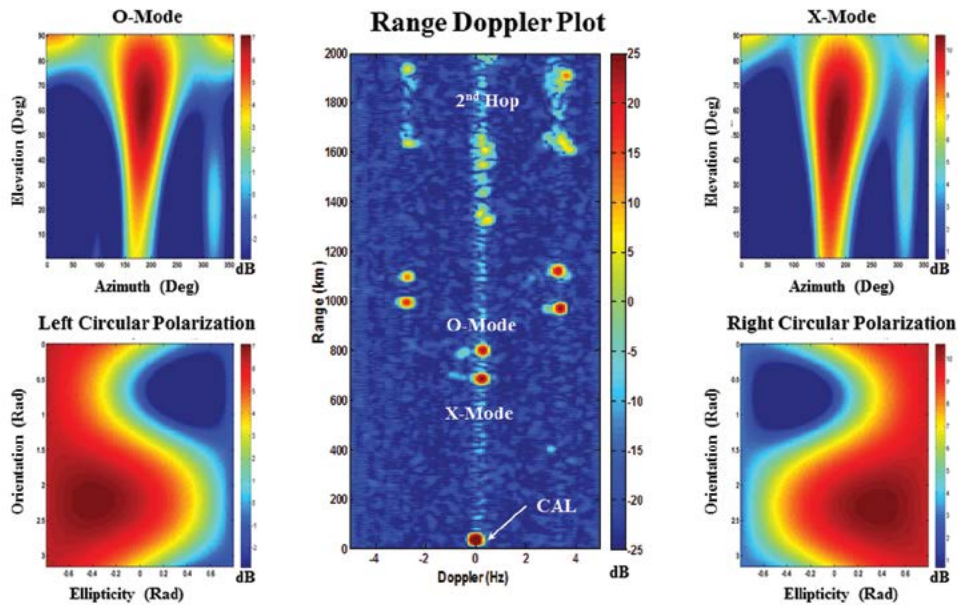


FIGURE 2 Experimental results demonstrate direction-of-arrival and polarization estimation by EMVS. Range Doppler plot (center) shows range separation of ordinary (O) and extraordinary (X) modes at each of three different sites offset in Doppler. The azimuth and elevation are estimated and plotted for the select ordinary and extraordinary modes (top left and top right, respectively). Polarization ellipticity and orientation angles are also estimated and plotted showing accurate left-hand circular and right-hand circular states for the select ordinary and extraordinary modes (bottom left and bottom right, respectively).

Processing: Field testing of the EMVS was conducted to verify the operational sensing capabilities of the EMVS antenna design (see Figs. 2 and 3). The bistatic transmit and receive setup is adopted with known linear frequency modulated chirp waveforms in order to collect single-hop ionospheric radar data. A local source at the receive site transmitting synchronized waveforms is used for calibration. The dataset is collected for a frequency at which the ionosphere supports two propagating modes that are distinguished by different refracted ionospheric heights.

The received electromagnetic signal can be modeled as having independent delay, spatial, and polarization components. Delay characteristics are often used to identify range and Doppler. Spatial components enable azimuthal and elevation signal direction-of-arrival estimation. The polarization component provides a means of measuring the orientation of the electric field vector, which for skywave signals means an added ability to separate ordinary and extraordinary propagating modes and mitigate Faraday fading effects.

Raw IQ (in-phase/quadrature) data is first range- and Doppler-processed at each channel. The local source signal is selected from the range-Doppler surface for calibration of the collected dwell. Due to different reflected ionospheric heights, the signal path delay resultant from differing propagation path distances produces a unique scenario whereby the ordinary or



FIGURE 3 Fielded EMVS setup on 5 ft tall stand with battery to power antenna "active balun" on ground plane at base.

extraordinary mode signals appear range separated. This is particularly useful for validation of EMVS polarization identification.

Selecting a skywave signal of interest, the polarization state is held constant while a coarse estimate of the azimuth and elevation for the signal is calculated.³ Approximate polarization ellipticity and orientation angles are then obtained by holding the spatial components constant and utilizing the coarse azimuth and elevation estimate. This process is performed once more for refined azimuth and elevation estimates.

Summary: In the preliminary datasets, target polarization aspect changes as well as temporal and spatial ionospheric dynamics are observed. The experimental results demonstrate angle-of-arrival and validate polarization estimation capability for ionospherically propagated HF signals. The structural stability of the EMVS has enabled data collections in a variety of environments including sun, rain, snow, and ice. Studies on the EMVS for accuracy of direction-of-arrival estimation and for improved noise mitigation techniques are ongoing.

[Sponsored by the Intelligence Advanced Research Projects Activity (IARPA)]

References

- ¹ A. Nehorai and E. Paldi, "Vector Sensor Processing for Electromagnetic Source Localization," Conference Record of the 25th Asilomar Conference on Signals, Systems and Computers, Pacific Grove, CA, 1991, pp. 566–572.
- ² A. Nehorai, K. Ho, and B.T.G. Tan, "Minimum-Noise-Variance Beamformer with an Electromagnetic Vector Sensor," *IEEE Trans. Sig. Proc.* **47**(3), 601–618 (1999).
- ³ W. Lee, M. Parent, and G. San Antonio, "EMVS Design and Characteristics," 2012 Allerton Antenna Applications Symposium.



Intrinsically Switched Varactor-Tuned Filters and Filter Banks

A.C. Guyette
Electronics Science and Technology Division

Introduction: Tunable filters are essential to the realization of frequency-agile microwave systems. They are particularly useful in receiver applications because they can be reconfigured to adapt to a changing electromagnetic environment, capturing signals of interest while blocking unwanted interferers. There is a need for both high-performance tunable *bandpass* and *bandstop* filters, depending on the configuration and the specific requirements of the system.¹

When designing a tunable filter, there are several performance trade-offs to be considered. For example, as the tuning range of a tunable filter is widened, it becomes increasingly difficult to maintain a good filter response across the entire tuning range. As the tuning range is increased, the tuning elements are necessarily coupled more tightly to the resonators, and so their loss has greater effect on the overall resonator unloaded Q (Q_u). Poor resonator Q_u results in a degradation of filter selectivity, as well as increased passband insertion loss in the case of bandpass filters and decreased stopband rejection in the case of bandstop filters.

In an attempt to extend the tuning range of tunable filters without degrading performance, switched-bank tunable filter configurations are often used. Switched tunable bandpass filter banks (Fig. 4(a)) and switched tunable bandstop filter banks (Fig. 5(a)) are comprised of a number of tunable filters with tuning ranges corresponding to bands within the desired full tuning range. To select the appropriate filter, RF switches are placed at the input and output in the bandpass bank, and before and after every filter in the bandstop bank. The result is superior performance, in terms of either total tuning range or passband insertion loss, to that which is possible with a single tunable filter. The switches themselves, however, add significant passband insertion loss, which tends to increase as the number of filters in the bank increases; this significantly diminishes or eliminates the insertion loss improvement provided by reducing the tuning range of each of the individual constituent filters. In addition, the switches increase the size, weight, power consumption, and control complexity, and they can degrade the linearity of the filter bank. NRL has developed a solution to this problem in the form of intrinsically switched tunable filters, wherein the switching function is performed by the filters themselves, thereby completely eliminating the need for switches in filter banks (Fig. 4(b) and Fig. 5(b)) and in other applications where a switchable filter is needed.

Intrinsically switched tunable filters² are tunable filters that are switched on and off using the same tuning elements that tune their center frequencies and/or bandwidths. In its "off" state, an ideal intrinsically switched bandpass filter rejects signals of all frequencies, and an ideal intrinsically switched bandstop filter passes signals of all frequencies. This is achieved by using the capacitive tuning elements (varactors) to control the voltage and current distributions in the resonators such that the electric and magnetic interresonator coupling coefficients are equal and opposite, resulting in zero net coupling. Intrinsically switched bandstop filters can be realized with bandstop sections consisting of two transmission paths, where the bandstop response is suppressed with constructive interference.

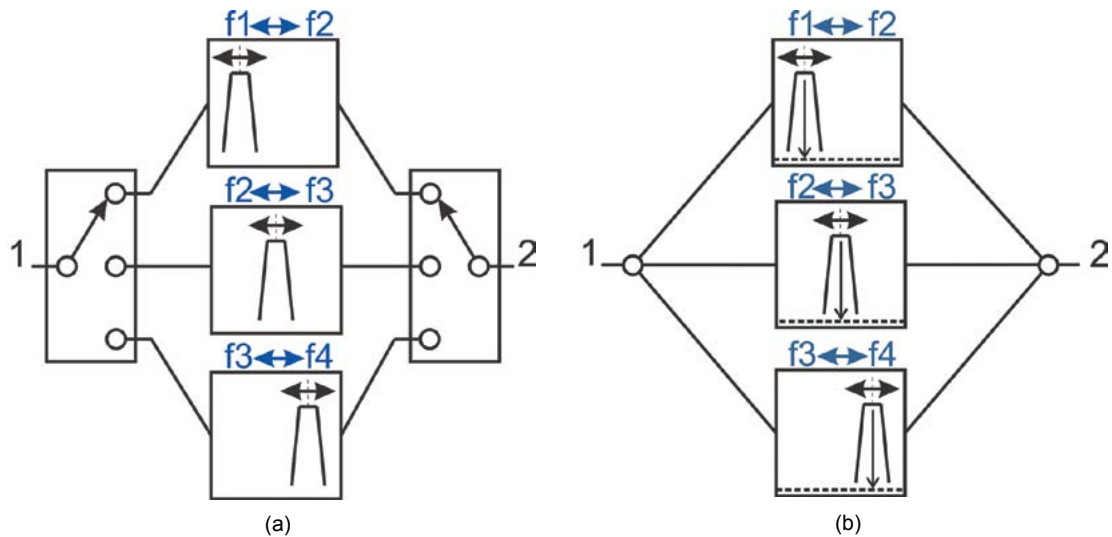


FIGURE 4 (a) Conventional switched tunable bandpass filter bank. (b) Switchless tunable bandpass filter bank using intrinsically switched tunable bandpass filters.

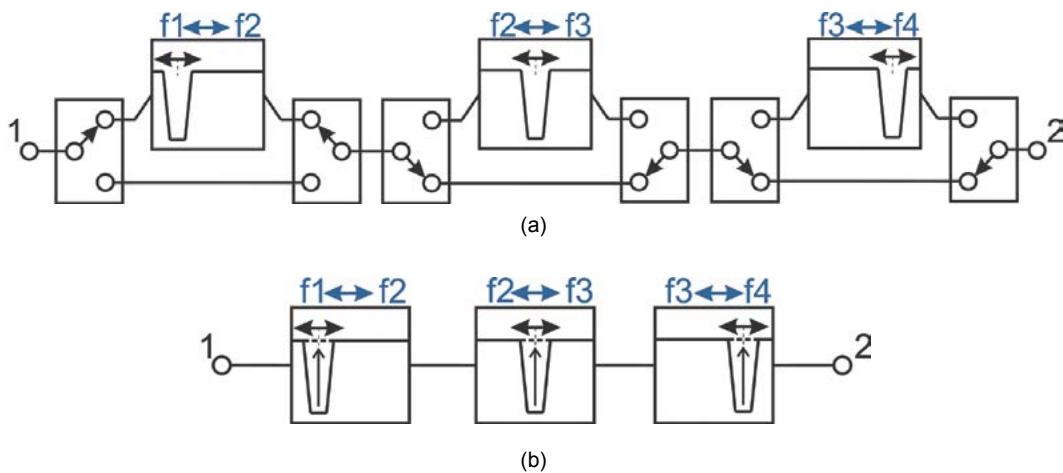


FIGURE 5 (a) Conventional switched tunable bandstop filter bank. (b) Switchless tunable bandstop filter bank using intrinsically switched tunable bandstop filters.

Intrinsically Switched Tunable Bandstop Filters:

A second-order intrinsically switched notch filter prototype is shown in Fig. 6(a). It consists of two intrinsically switched bandstop sections in cascade, with a small amount of coupling introduced between the two resonators, which has the effect of significantly increasing the notch depth by adding a small amount of destructive interference.³ Design and simulation were conducted using a combination of circuit and electromagnetic simulation software. The substrate is Rogers Duroid RO4003 and the varactors are commercially available hyper-abrupt varactors. Shown in Fig. 6(b) and Fig. 6(c) are the simulated and measured results. In the intrinsic-off state measurement, the resonators

are tuned to 725 MHz but the bandstop response is completely suppressed.

Intrinsically Switched Tunable Bandpass Filter Bank:

An intrinsically switched tunable bandpass filter bank microstrip prototype was designed, built, and tested to demonstrate the feasibility of an intrinsically switched filter bank. The prototype (Fig. 7(a)) is comprised of three third-order intrinsically switched bandpass filters (filters A, B, and C) coupled to short-circuit-terminated transmission-line manifolds at the input and output. The substrate is Rogers Duroid RO4003 and the varactors are commercially available hyper-abrupt varactors. Only five unique control volt-

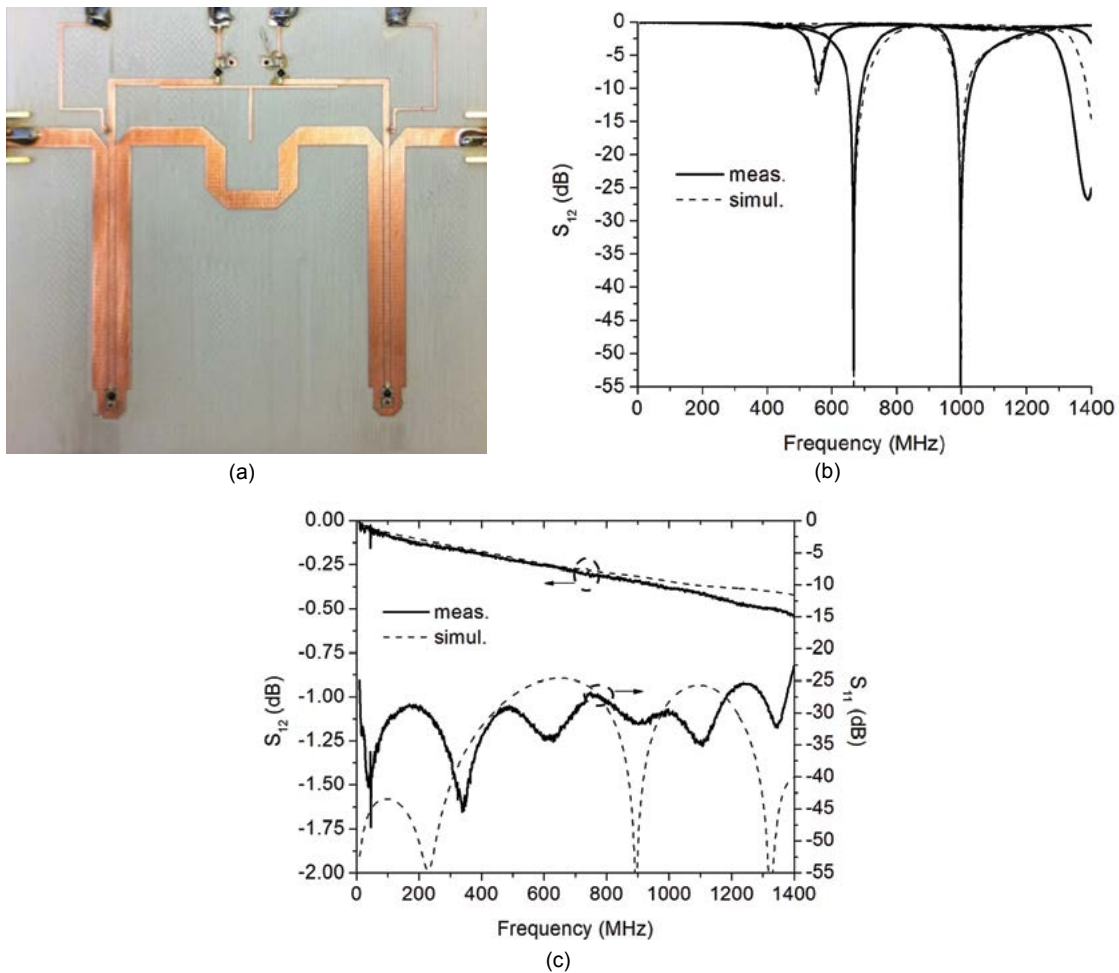


FIGURE 6 Intrinsic switched tunable notch filter prototype: (a) fabricated circuit (overall dimension 8.6 cm × 8.1 cm), (b) center frequency tuning, and (c) intrinsic off state. S_{11} = reflection, S_{12} = transmission.

ages are needed for standard operation. The passband bandwidth is a constant 50 MHz, with more than 40 dB of isolation between filters. Shown in Fig. 7(b) are measurements showing the full composite tuning range, and shown in Fig. 7(c) are simulated and measured results with all three filters on simultaneously. The intrinsically switched bank approach removes the switch-loss-imposed upper limit to the number of filters that can be used; so realizing low-loss tunable filter banks comprised of large numbers of low-loss narrow-tuning-range filters becomes a problem of manifold design rather than the much more difficult problem of realizing low-loss high-throw or cascaded switches.

Summary: NRL has developed a new class of reconfigurable RF device called intrinsically switched tunable filters. It is expected that intrinsically switched tunable filters and filter banks will play an important role in the realization of future high-performance microwave systems.

[Sponsored by ONR]

References

- ¹ P. Wong and I. Hunter, "Electronically Tunable Filters," *IEEE Microwave Magazine* **10**, 46–54 (2009).
- ² A.C. Guyette, "Intrinsically Switched Varactor-Tuned Filters and Filter Banks," *IEEE Trans. Microwave Theory Tech.* **4**, 1044–1056 (2012).
- ³ D.R. Jachowski, "Compact, Frequency-Agile, Absorptive Bandstop Filters," 2005 *IEEE MTT-S International Microwave Symposium Digest*, pp. 513–516, June 2005.

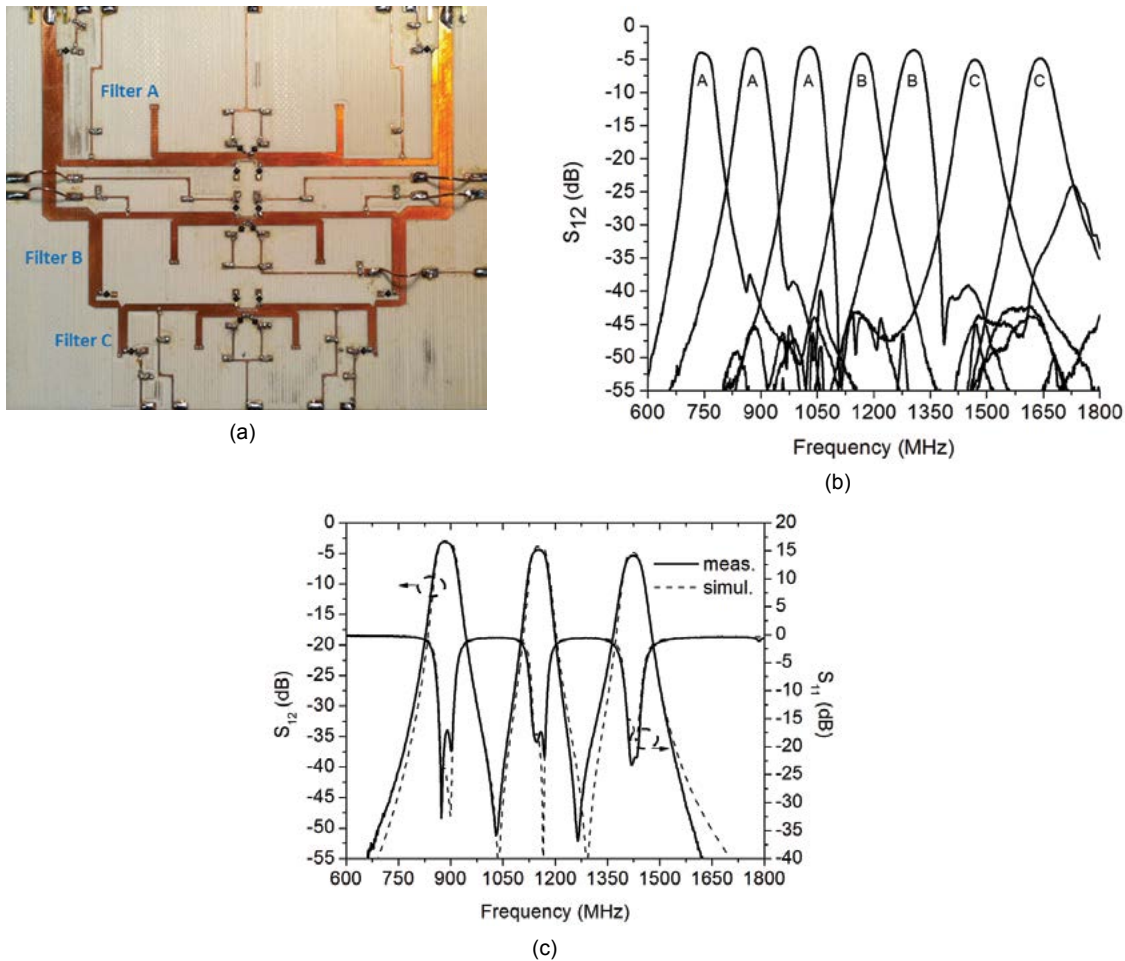


FIGURE 7
 Intrinsic switched tunable bandpass filter bank prototype: (a) fabricated circuit, (b) measured full tuning range, (c) all filters on simultaneously. S_{11} = reflection, S_{12} = transmission.

Thermoelectroelastic Simulation of GaN Devices

M.G. Ancona,¹ S.C. Binari,² and D.J. Meyer¹

¹Electronics Science and Technology Division

²Electronics Science and Technology Division, retired

Introduction: Because of the large bandgap and high electrical conductivity of the semiconductor GaN, electronic devices based on this material are playing an increasingly indispensable role in Navy applications in RF electronics, power electronics, and solid-state lighting. To understand the operation, performance, and reliability of these devices, it is crucial that one take into account GaN's electroelastic and thermoelastic properties, its strong spontaneous polarization, its built-in strains, and the coupling of these phenomena to the electron transport. From a theoretical perspective, all these interactions are well understood, but heretofore

they had been studied in detail only in simplified one-dimensional cases, and not in realistic device geometries. The work reviewed here^{1,2} developed a numerical simulation code that solves the complete thermoelectromechanical equations in multi-dimensions and thereby allows a variety of important GaN devices to be fully analyzed for the first time. Especially relevant application areas include the design of scaled GaN transistors for high frequency operation and the physics of their failure. Through such uses, this advanced simulator is likely to impact Navy-relevant applications such as solid-state radar and electric ship power distribution, as well as the larger GaN research and development community.

Theory and Numerics: GaN and its alloys with indium and aluminum are unique among the technologically important semiconductors in being strongly piezoelectric. As a result, full quantitative analyses of electronic devices made of these materials must include

the mechanical degrees of freedom. That GaN applications often involve high temperatures means thermal coupling should be modeled also. And since all device situations are inhomogeneous, usually in 2D but sometimes 3D, a multidimensional capability is essential. To incorporate all this physics in a tractable fashion, a continuum approach was used in which the system is described by five coupled partial differential equations plus five crucial constitutive equations and a consistent set of boundary conditions. The solutions consist of the electric potential, the electron density and current, the stress/strain, and the temperature as functions of position and time.

The governing equations are solved in geometries and with material properties set by the particular device being modeled. In our work we have focused on high electron mobility transistor (HEMT) structures of varying geometries. The equations are programmed and solved for both DC and small-signal AC conditions within COMSOL's general finite-element program.³ Finally, the run-time of the simulations was greatly improved by exploiting the 2D nature of the devices of most interest and by solving the electron transport equations (which require a fine mesh) only in small "device regions" near the contacts.

Application – RF Devices: The simulated current-voltage (I - V) curves for a standard GaN HEMT are plotted in Fig. 8(a) and they look very much like those measured experimentally (e.g., in Ref. 4). Using the ability of numerical simulation to look inside a working device, we plot in Figs. 8(b-d) solution profiles under ON-state conditions. Of note is the fact that the peak mechanical stresses, while quite high (~ 3.5 GPa), are well below the yield strengths of these materials.

Application – Transistor Reliability: GaN HEMTs are known to fail by apparently mechanical means, with grooves, pits, and cracks often appearing during accelerated life testing.⁵ An intriguing hypothesis about these failures is that they are triggered by piezoelectric stress,⁵ and to investigate this we examine solutions under high-power conditions with drain voltage $V_D = 20$ V and gate voltage $V_G = 0$. The simulated channel temperature (Fig. 9(a)) is very high (~ 400 °C), and this would surely accelerate any degradation processes. The electric field (Fig. 9(b)) is also quite high at the drain corner of the channel and this would undoubtedly lead to significant electron injection. But the mechanical stresses (Fig. 9(b)) do seem not especially elevated (< 5 GPa), and half of the peak stress comes not from the piezoelectric contribution but from thermal stresses.

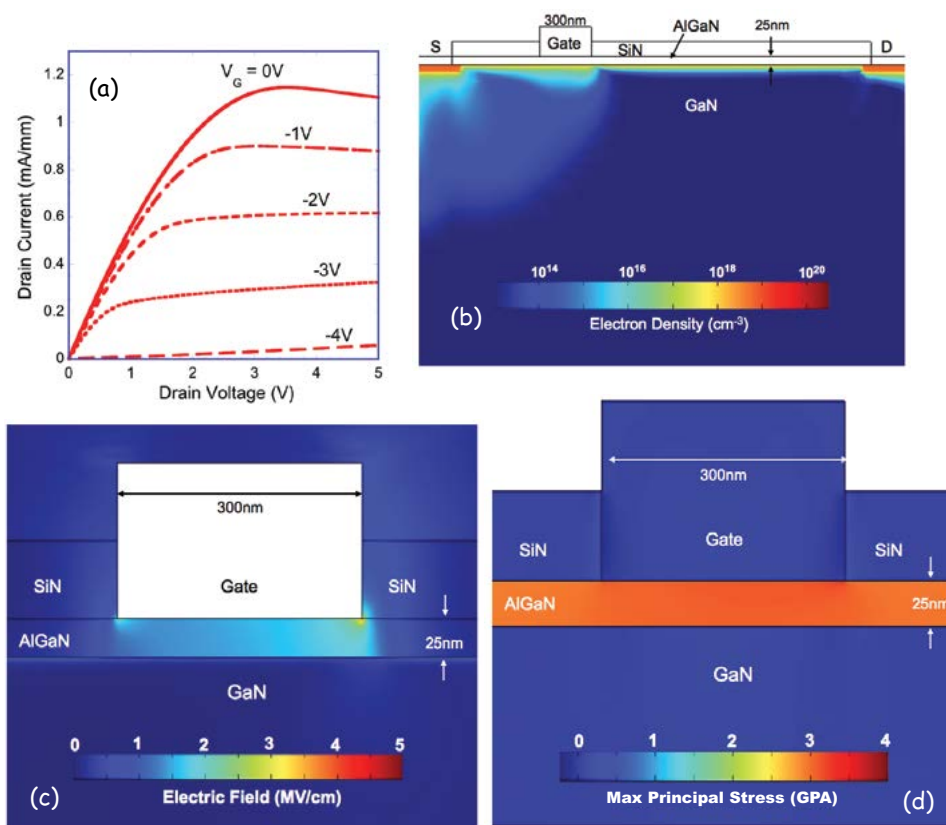


FIGURE 8 Simulated (a) I - V curves for a standard GaN HEMT, and plots of its (b) electron density, (c) electric field, and (d) principal stress in the ON-state ($V_G = 0$ V, $V_D = 5$ V).

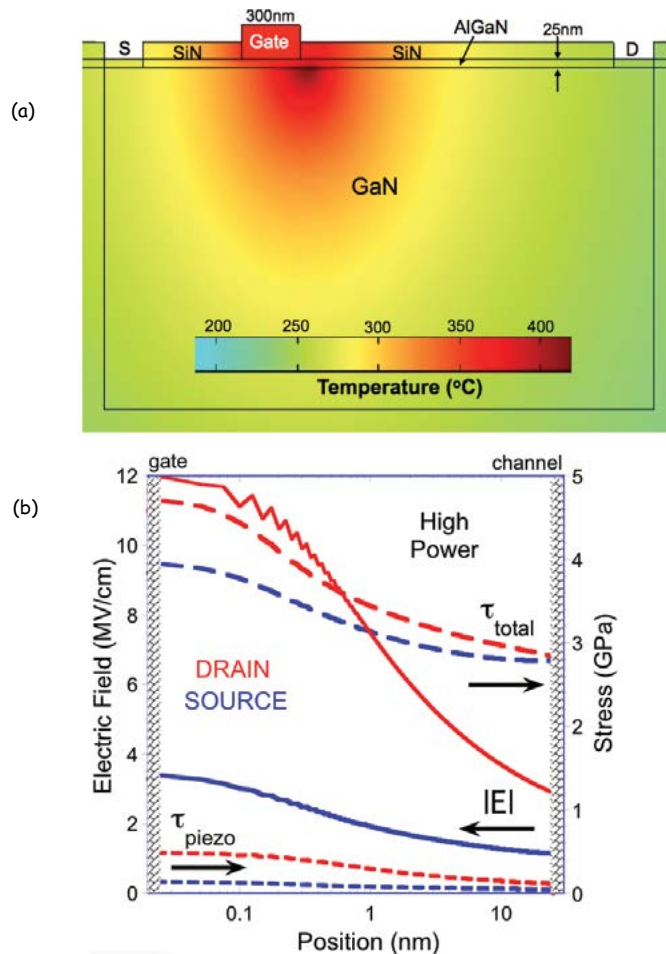


FIGURE 9 Simulated (a) temperature field and (b) electric field, piezoelectric stress, and total stress profiles across the AlGaN at the source/drain-side corners of the gate under high-power conditions.

A further set of simulations looked at the stress-concentrating effect of a crack (Fig. 10(a)), the effects of the crack's radius of curvature and depth on the stress concentration (Fig. 10(b)), and the impact that a crack can have on the drain characteristics (Fig. 10(c)).

Application – Transistor Scaling: To reach higher frequencies, a variety of scaled HEMT designs are being investigated with gate lengths below 100 nm. Of particular interest are the stresses introduced by gate structures and by regrown InGaN/InN source/drain contacts.⁶ Modeling is especially valuable for the scaled devices because as the geometrical size is reduced, the strain fields become increasingly multidimensional and the inhomogeneous mechanics plays an ever larger role in setting important device parameters such as the threshold voltage.

Summary: A numerical simulation code was developed that solves the complete thermoelectromechanical

equations describing piezoelectric semiconductors in multi-dimensions.^{1,2} The code was applied to a variety of important GaN devices, and for the first time allows for their full analysis.

[Sponsored by ONR]

References

- ¹ M.G. Ancona, S.C. Binari, and D.J. Meyer, "Fully Coupled Thermoelectromechanical Analysis of GaN High Electron Mobility Transistor Degradation," *J. Appl. Phys.* **111**, 074504 (2012).
- ² M.G. Ancona, "Fully Coupled Thermoelectroelastic Simulations of GaN Devices," 2012 IEEE International Electron Devices Meeting, San Francisco, CA; doi:10.1109/IEDM.2012.6479037.
- ³ www.comsol.com.
- ⁴ S.C. Binari, K. Ikossi, J.A. Roussos, W. Kruppa, D. Park, H.B. Dietrich, D.D. Koleske, A.E. Wickenden, and R.L. Henry, "Trapping Effects and Microwave Power Performance in Al-GaN/GaN HEMTs," *IEEE Trans. Electron. Devices* **48**(3), 465–471 (2001).
- ⁵ U. Chowdhury, J.L. Jimenez, C. Lee, E. Beam, P. Saunier, T. Balistreri, S.-Y. Park, T. Lee, J. Wang, M.J. Kim, J. Joh, and J.A. del Alamo, "TEM Observation of Crack- and Pit-Shaped Defects in Electrically Degraded GaN HEMTs," *IEEE Electron. Device Lett.*

29(10), 1098–1100 (2008).

⁶ U. Singiseti, M.H. Wong, S. Dasgupta, Nidhi, B. Swenson, B.J. Thibeault, J.S. Speck, and U.K. Mishra, “Enhancement-Mode N-Polar GaN MISFETs With Self-Aligned Source/Drain Regrowth,” *IEEE Electron Device Lett.* **32**(2), 137–139 (2011).

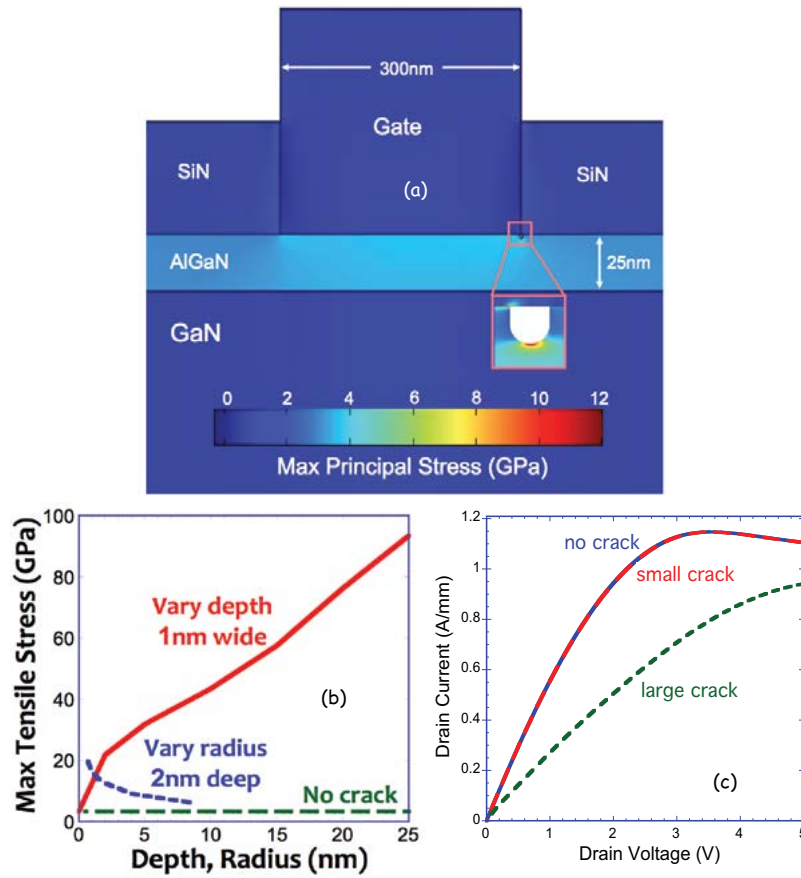


FIGURE 10

Simulations of a damaged AlGaIn/GaN HEMT with a “crack” at the drain-side corner of the gate and showing (a) the stress concentration effect, the dependence of the peak stress on (b) the radius of curvature and depth of the crack, and (c) the effect of small and large cracks on the drain characteristics.

